RESEARCH ARTICLE

Performance Evaluation of ETo Prediction Methods: Dispersion Analysis and Accuracy Criteria Across Time Intervals

Mostafa Sadeghzadeh[1,*], **Jalal Shiri**[1,2] and **Sepideh Karimi**[1]

[1] Water Engineering Department, Faculty of Agriculture, University of Tabriz, Tabriz, Iran
[2] Water Engineering and Science Research Institute (WESRI), University of Tabriz, Tabriz, Iran

Abstract

Accurate forecasting of reference evapotranspiration (ET_o) is essential for sustainable water resource management and precision agriculture, yet systematic comparisons across extended forecasting horizons remain limited. This study evaluates three ET_o prediction methods—Random Forest (RF), Cartesian Genetic Programming (CGP), and Convolutional Neural Network accelerated by Graphics Processing Unit (CNN-GPU)—across six time intervals ranging from 1 to 364 days, using data from two semi-arid stations in northwestern Iran. Model performance was assessed via dispersion analysis (scatter and violin plots) and four accuracy metrics (RMSE, MAE, R^2, SI). Results indicate that RF and CNN-GPU consistently outperform CGP, particularly at extended horizons. At the 364-day interval, CNN-GPU achieved the highest accuracy (RMSE: 0.678 mm/day, R^2: 0.874), while RF maintained robust and stable performance (RMSE: 0.683 mm/day, R^2: 0.872, SI: 0.244–0.278). CGP exhibited comparatively higher error at extended horizons (RMSE: 0.702 mm/day at 364 days) and greater prediction variability. Statistical validation via two-sample t-tests, F-tests, and ANOVA confirmed significant inter-method differences at lags of 22 days and beyond ($p < 0.05$), with CNN-GPU frequently demonstrating superior accuracy at longer timescales. Time-series analyses further confirmed that RF and CNN-GPU effectively capture seasonal ET_o patterns, whereas CGP exhibits increasing error dispersion with lag. All methods produced physically inconsistent negative lower-bound predictions, identifying a shared limitation requiring post-processing or architectural constraints in operational deployment.

Keywords: ET_o prediction, random forest, CNN-GPU, genetic programming, dispersion analysis, time intervals.

1 Introduction

Reference evapotranspiration (ET_o), an important parameter in agricultural water management, represents the evaporative demand of the atmosphere independent of crop type, growth stage, or

Submitted: 06 May 2025
Accepted: 25 August 2025
Published: 15 September 2025

Vol. 2, **No.** 3, 2025.
10.62762/TETAI.2025.125348

***Corresponding author:**
✉ Mostafa Sadeghzadeh
sadeqzadeh.m@gmail.com

Citation
Sadeghzadeh, M., Shiri, J., & Karimi, S. (2025). Performance Evaluation of ETo Prediction Methods: Dispersion Analysis and Accuracy Criteria Across Time Intervals. *ICCK Transactions on Emerging Topics in Artificial Intelligence*, 2(3), 182–191.

© 2025 by the Authors. Published by Institute of Central Computation and Knowledge. This is an open access article under the CC BY license (https://creativecommons.org/licenses/by/4.0/).

management practices. Allen et al. [1] argued that the Penman-Monteith equation adopted by FAO can serve as a reference standard formula for ET_o estimation under wide climatic conditions. This model closely aligns with spatial and temporal climatic patterns in regions with varying elevations and climates, emphasizing its adaptability [2]. Accurate ET_o prediction is critical for irrigation planning, water resource allocation, and sustainable agricultural practices, especially in regions with limited water resources [3, 4]. Given the impact of climate change on precipitation patterns and increasing temperatures, accurate ET_o prediction is becoming increasingly important to mitigate drought impacts and ensure food security [5].

Traditional methods such as the Penman-Monteith equation require extensive meteorological data that are not always available. So, various models relying on fewer input variables have been developed for ET_o calculation. In recent years, machine learning (ML)-based techniques have gained popularity for ET_o estimation, with methods ranging from linear genetic programming to support vector machines demonstrating competitive accuracy against physics-based approaches [6, 7]. Among these methods, genetic programming (GP) and random forest have shown promising results and have been widely applied in this context [8, 9]. Further, deep learning techniques, especially convolutional networks (CNNs), have been employed for predicting ET_o with limited input data [10, 11].

Genetic programming evolves computer programs to perform user-defined tasks [12]. In the context of ET_o prediction, GP has been used to develop empirical models that relate meteorological variables to ET_o [6, 9]. Different variants of GP, such as grammatical evolution (GE), Cartesian genetic programming (CGP), and multi-objective genetic programming (MOGP), have been investigated to improve prediction accuracy and model interpretability; continuous CGP representations in particular have demonstrated competitive performance in complex function approximation and multi-objective optimization contexts [13, 14]. For example, gene expression programming (GEP) has been successful in predicting ET0 under different climate conditions due to its ability to produce simple and accurate models [15].

Random forest (RF) is an ensemble learning method that builds multiple decision trees and combines their predictions to improve accuracy and reduce overfitting [16]. The ability of RF to handle large datasets and capture complex nonlinear interactions between variables makes it particularly suitable for regression tasks involving structured time-series inputs [17, 18].

Despite significant progress in ML-based models for ET_o prediction, comprehensive comparisons across diverse forecasting horizons remain limited, particularly for long-term predictions. Existing research has predominantly focused on short-term forecasts, often overlooking the accuracy and reliability of models over extended timescales. Moreover, the performance of GP variants, such as Cartesian GP (CGP), has not been thoroughly benchmarked against established ML-based techniques. This study addresses these gaps by evaluating three ET_o prediction methods, namely, RF, CGP, and CNN-GPU across timescales ranging from 1 to 364 days. Through dispersion analysis (scatter and violin plots), accuracy metrics (RMSE, MAE, R^2, SI), statistical validation (t-tests, F-tests, ANOVA), and time-series analysis, a detailed assessment of the models' performances were provided, with a particular emphasis on long-term forecasting capabilities.

2 Material and methods

2.1 Climatic characteristics and ET_o patterns of the study area

Data from two counties of Meshkinshahr and Ahar, located in Ardabil and East Azerbaijan provinces, Iran were utilized to evaluate the proposed methodologies. This region has a semi-arid and mountainous climate, with an average annual rainfall of about 300 to 400 mm and an average annual temperature of $12°C$ (see Figure 1). The ET_o series shown in Figure 1 represents the average ET_o calculated for the two study areas, Meshkinshahr and Ahar. This series reflects the mean ET_o values of these two locations and is plotted to provide a general overview of evapotranspiration patterns in the study region.

Daily ET_o data were collected from a meteorological station for the period 1 January 2015 to 20 March 2023. The data included ET_o values calculated using the standard FAO Penman-Monteith method, derived from meteorological variables e.g. air temperature, relative humidity, wind speed and solar radiation [9].

$$ET_o = \frac{0.408\Delta(R_n - G) + \gamma\frac{900}{T+273}u_2(e_s - e_a)}{\Delta + \gamma(1 + 0.34u_2)} \quad (1)$$

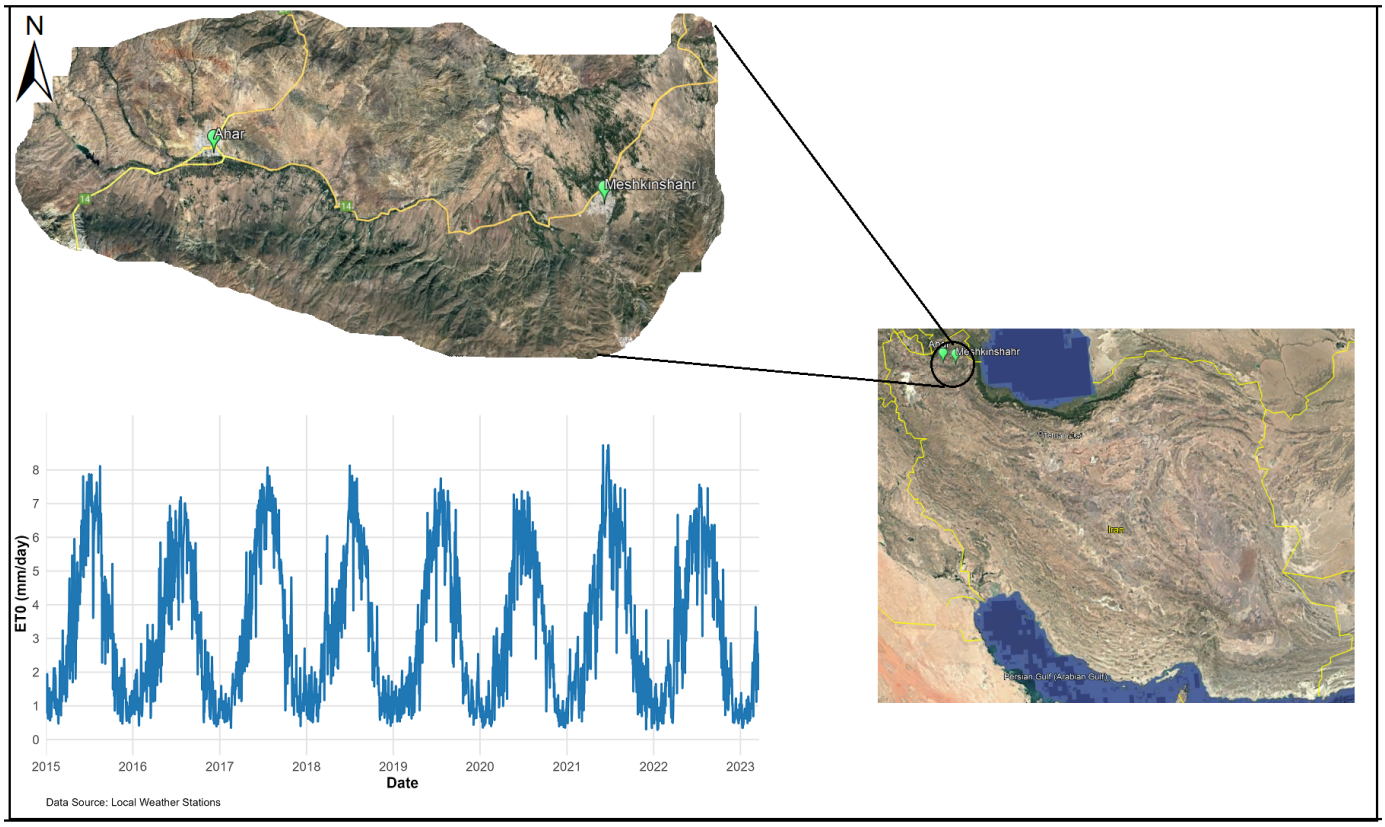


Figure 1. Study area and average ET_o time series.

In this formula, ET_o stands for the reference evapotranspiration (mmd^{-1}) and R_n is the net solar radiation at the vegetative surface (MJ $m^{-2}d^{-1}$). G is the soil heat flux (MJ $m^{-2}d^{-1}$), T denotes the mean air temperature ($°C$), u_2 shows the wind speed at two meters above the ground (m/s), e_a and e_s represent the actual and saturated vapor pressures, respectively (kPa), Δ is the slope of the vapor pressure curve (kPa/$°C$), and γ shows the psychrometric constant (kPa/$°C$).

2.2 Overview of CGP, RF, and CNN-GPU

2.2.1 Cartesian Genetic Programming (CGP)

Cartesian Genetic Programming (CGP) employs a straightforward integer-based genetic representation of programs, structured as directed graphs [19]. These graph-based representations are highly versatile, supporting both cyclic and acyclic structures, and are applicable to diverse domains. Numerous studies have demonstrated that CGP outperforms other GP techniques in efficiency, while its simplicity facilitates its implementation [20, 21].

2.2.2 Random Forest (RF)

Random Forest (RF), a powerful ensemble learning approach, amplifies the predictive capability of multiple weak learners through a collective decision-making process, demonstrating strong performance in high-dimensional regression tasks where complex nonlinear relationships between input features and target variables must be captured [22]. Introduced by Leo Breiman [16] in 2001, RF generates a series of unpruned classification or regression trees, each constructed from randomly sampled training data and feature subsets. The ensemble's predictions are synthesized via majority voting for classification tasks or averaging for regression tasks. RF demonstrates remarkable efficacy in datasets with a high number of variables relative to observations, making it a versatile tool for diverse, large-scale computational challenges. Its adaptability to specialized learning tasks and its capacity to evaluate variable significance further enhance its utility [16, 23]. By integrating numerous randomized decision trees and consolidating their outputs, RF delivers exceptional accuracy and robustness, establishing it as a cornerstone method in machine learning research.

2.2.3 CNN-GPU model for ET_o prediction

ET_o prediction was performed using CNN and accelerated by graphics processing units (GPU).

The CNN model was designed to process time series data, especially meteorological variables affecting ET_o, leveraging the hierarchical feature extraction capabilities that characterize convolutional architectures in deep learning [24]. The architecture consisted of multiple one-dimensional convolutional layers with ReLU activation and max pooling layers to extract local features. The output was passed to fully connected layers to produce the final forecast. The model was trained with historical data and the mean square error was minimized with the Adam optimizer. Key equations involved in the convolution operation:

$$y_t = \max\left(0, \sum_{i=0}^{k-1} w_i x_{t+i} + b\right) \quad (2)$$

where y_t is output at time t after applying the ReLU activation function, ReLU is modified linear unit activation function, k is Kernel size (number of filter weights), w_i is weight of the filter in position, x_{t+i} is input value at time $t + i$ and b is bias added to the weighted sum. The CNN model was implemented using the TensorFlow framework in Python with the Keras API, and the computations were accelerated on a GPU-accelerated system. The training process for the entire dataset took approximately 15 minutes at all time intervals. To quantify the performance gain, the same training process was run on a standard CPU. The CPU-based training took more than 60 minutes, indicating that GPU acceleration provides a performance speedup of over 5 times. GPU-accelerated training has been shown to provide substantial computational speedups for convolutional networks processing meteorological time series [10, 11], consistent with the observed 5× reduction in training time relative to CPU-based computation.

2.3 Evaluation Criteria

The performances of the applied models were evaluated using the following indices:

$$\text{RMSE} = \sqrt{\frac{1}{N}\sum_{i=1}^{N}\left(ET_{o,i}^{\text{observed}} - ET_{o,i}^{\text{predicted}}\right)^2} \quad (3)$$

$$MAE = \frac{1}{n}\sum_{i=1}^{n}|ETo_{predicted,i} - ETo_{observed,i}| \quad (4)$$

$$\text{SI} = \frac{\text{RMSE}}{E\overline{T}_o} \quad (5)$$

where ET_o^{observed} and $ET_o^{\text{predicted}}$ are the observed and predicted values, respectively and $E\overline{T}_o$ is average ET_o value over the study period.

2.4 Model development

The data were split into training and test sets in a ratio of 80-20. For each forecast interval (lags 1, 11, 22, 91, 181, and 364 days), input matrices were constructed using ET_o values at times past the specified lag. Specifically, for a lag i, the input variables consisted of ET_o values at times $t-k$ where $k \leq i$. Each method was trained on the training set and evaluated on the test set. To ensure the robustness of the results, Monte Carlo simulations with 1000 iterations were performed to estimate 95% confidence intervals [25].

2.5 Statistical analyses

To examine statistical differences between methods, two-sample t-tests and F-tests were performed to compare means and variances of predictions in pairs, following standard parametric statistical procedures for comparing model outputs [26]. Also, analysis of variance (ANOVA) was performed to assess overall differences between methods at each lag. These tests were performed at a significance level of 0.05 to identify significant differences. Figure 2 presents the schematic flowchart of the present research.

3 Results and discussion

3.1 Performance evaluation of ET_o prediction methods: dispersion analysis and accuracy criteria in different time intervals

The evaluation results are presented in Figure 3 and Table 1. Figure 3 shows scatter plots of predicted and target ET_o values for the adopted time intervals (1, 11, 22, 91, 181, and 364 days). To provide context for the model configurations, a network with 100 nodes and up to 10 levels of recurrence, with a population of 500 and 50 generations was used for the CGP model. Further, RF regressor in the scikit-learn library was used with 100 trees (n_estimators=100) and a random seed of 42 for repeatability.

In Figure 3, each chart is plotted with a 1:1 reference line (solid line); points positioned nearer to this line represent more accurate predictions. At shorter lags

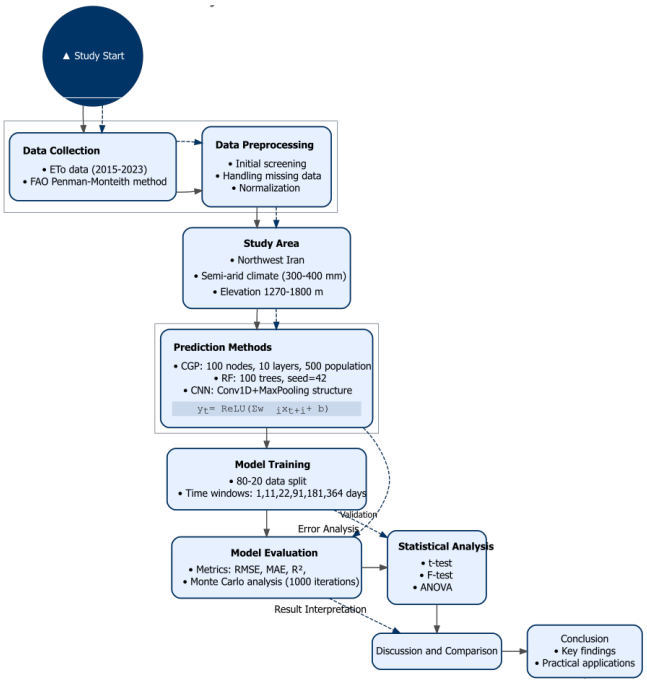


Figure 2. Schematic diagram of research stages.

Table 1. Performance evaluation criteria for RF, CGP, and CNN-GPU models.

Method	Lag	RMSE	MAE	R^2	SI
RF	1	0.803	0.577	0.835	0.278
CGP	1	0.708	0.494	0.872	0.245
CNN-GPU	1	0.706	0.502	0.872	0.244
RF	11	0.735	0.523	0.861	0.255
CGP	11	0.713	0.491	0.869	0.247
CNN-GPU	11	0.694	0.492	0.876	0.241
RF	22	0.711	0.502	0.870	0.247
CGP	22	0.704	0.486	0.873	0.244
CNN-GPU	22	0.710	0.525	0.871	0.246
RF	91	0.687	0.488	0.875	0.244
CGP	91	0.701	0.481	0.870	0.249
CNN-GPU	91	0.694	0.508	0.873	0.246
RF	181	0.688	0.489	0.868	0.253
CGP	181	0.704	0.482	0.862	0.259
CNN-GPU	181	0.707	0.535	0.861	0.260
RF	364	0.683	0.484	0.872	0.259
CGP	364	0.702	0.477	0.865	0.266
CNN-GPU	364	0.678	0.501	0.874	0.257

(1, 11, and 22 days), the points for all methods are generally close to the 1:1 line with minimal scatter. CNN-GPU (turquoise) and RF show slightly tighter clustering compared to CGP at these lags, with CNN-GPU appearing to have the least scatter at lag 1 day. As the lag increases to 91, 181, and 364 days, the scatter of points increases slightly for all methods, but they remain relatively close to the 1:1 line. At longer lags, RF and CNN-GPU continue to show less deviation compared to CGP, which exhibits slightly more scatter, especially at 364 days interval.

Table 1 summarizes the evaluation metrics (RMSE, MAE, R^2, and SI) for each method across different prediction intervals. For the 1-day prediction, CNN-GPU achieves the best performance with an RMSE of 0.706 and R^2 of 0.872, whereas RF yields a higher RMSE of 0.803 and R^2 of 0.835. At 11 days, CNN-GPU again outperforms other methods with an RMSE of 0.694 and R^2 of 0.876, while RF records an RMSE of 0.735. For the 22-day horizon, RF and CNN-GPU produce nearly identical results, with RMSE values of 0.711 and 0.710, respectively. In contrast, at 91 days, RF delivers the most accurate predictions, achieving an RMSE of 0.687 and R^2 of 0.875, compared to CGP with an RMSE of 0.701. At 181 days, RF continues to lead with an RMSE of 0.688 and R^2 of 0.868, while CNN-GPU shows a slightly higher RMSE of 0.707. Finally, for the 364-day interval, CNN-GPU provides the best performance with an RMSE of 0.678 and R^2 of 0.874, whereas CGP records the highest RMSE of 0.702. The SI metric further indicates that all methods exhibit low relative dispersion, with CNN-GPU achieving the lowest SI at shorter horizons (e.g., 0.241 at 11 days) and RF maintaining lower dispersion at longer horizons (e.g., 0.244 at 91 days).

Overall, RF and CNN-GPU perform consistently across all prediction intervals, with CNN-GPU showing a slight edge at shorter lags (1 and 11 days) and RF performing better at intermediate lags (91 and 181 days). At the longest intervals (364 days), CNN-GPU again outperforms the others. CGP performs competitively but shows slightly more scatter at longer prediction intervals (e.g., 364 days). These results suggest that both RF and CNN-GPU are reliable for ET_o prediction across various time intervals, with CNN-GPU being particularly effective at shorter and very long lags.

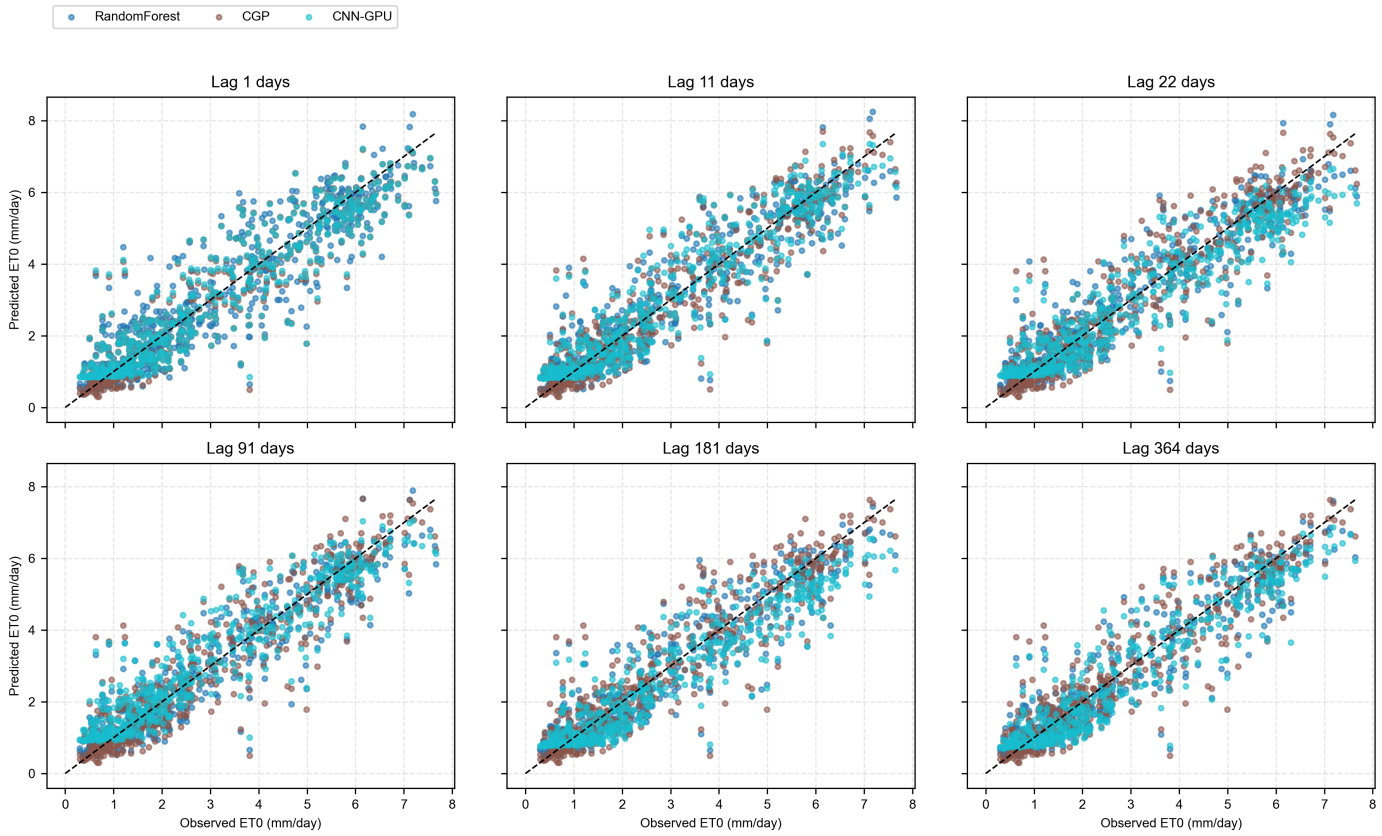


Figure 3. Scatter plots of ET_o forecasts over different time periods.

3.2 Comparison of ET_o prediction time series for different methods at different lags

Figure 4 shows the predicted versus target ET_o values. At shorter intervals (1, 11, and 22 days), all methods closely follow the trend of the observed values, with minimal deviation at the extreme points. CNN-GPU and RF show slightly better alignment with the observed data compared to CGP, especially at lag 1 day. As the intervals increase to 91, 181, and 364 days, the predictions of all methods remain relatively close to the observed values, though slight deviations become more noticeable at the extreme points. RF and CNN-GPU continue to track the target data more closely than CGP, which shows slightly larger deviations at longer intervals, particularly at 364 days interval.

3.3 Statistical analysis of significant differences in the performance of ET_o prediction models using t and F tests

Figure 5 shows a bar graph of the statistical differences between pairs of ET_o prediction methods using t-tests and F-tests. The statistics are displayed on the left y-axis, and the p-values are shown in logarithmic form (-log10) on the right y-axis. The significance threshold line (p=0.05, equivalent to -log10(p)=1.3) can be inferred for interpretation.

3.4 Overall evaluation of statistical analysis for ET_o models

Statistical analysis using t-tests, F-tests, and ANOVA was conducted to assess significant differences in the performance of RF, CGP, and CNN-GPU across six prediction intervals (1, 11, 22, 91, 181, and 364 days). At shorter lags (1 and 11 days), t-tests and F-tests revealed no significant differences between the methods, with p-values consistently above 0.05 (e.g., ANOVA p-values of 0.438 and 0.206, respectively), indicating comparable performance and variance among the models. However, starting at 22 days, significant differences emerged, particularly involving CNN-GPU. For instance, at 22 days, t-tests showed significant differences for RF vs. CNN-GPU (p=0.0056) and CGP vs. CNN-GPU (p=0.0075), with ANOVA confirming overall significance (p=0.0071). This trend intensified at longer lags (91, 181, and 364 days), where CNN-GPU frequently outperformed others, as evidenced by highly significant t-test results (e.g., p=4.86E-07 for CGP vs. CNN-GPU at 181 days) and ANOVA p-values as low as 1.18E-05 (91 days) and 2.02E-06 (181 days). Notably, RF vs. CGP showed no

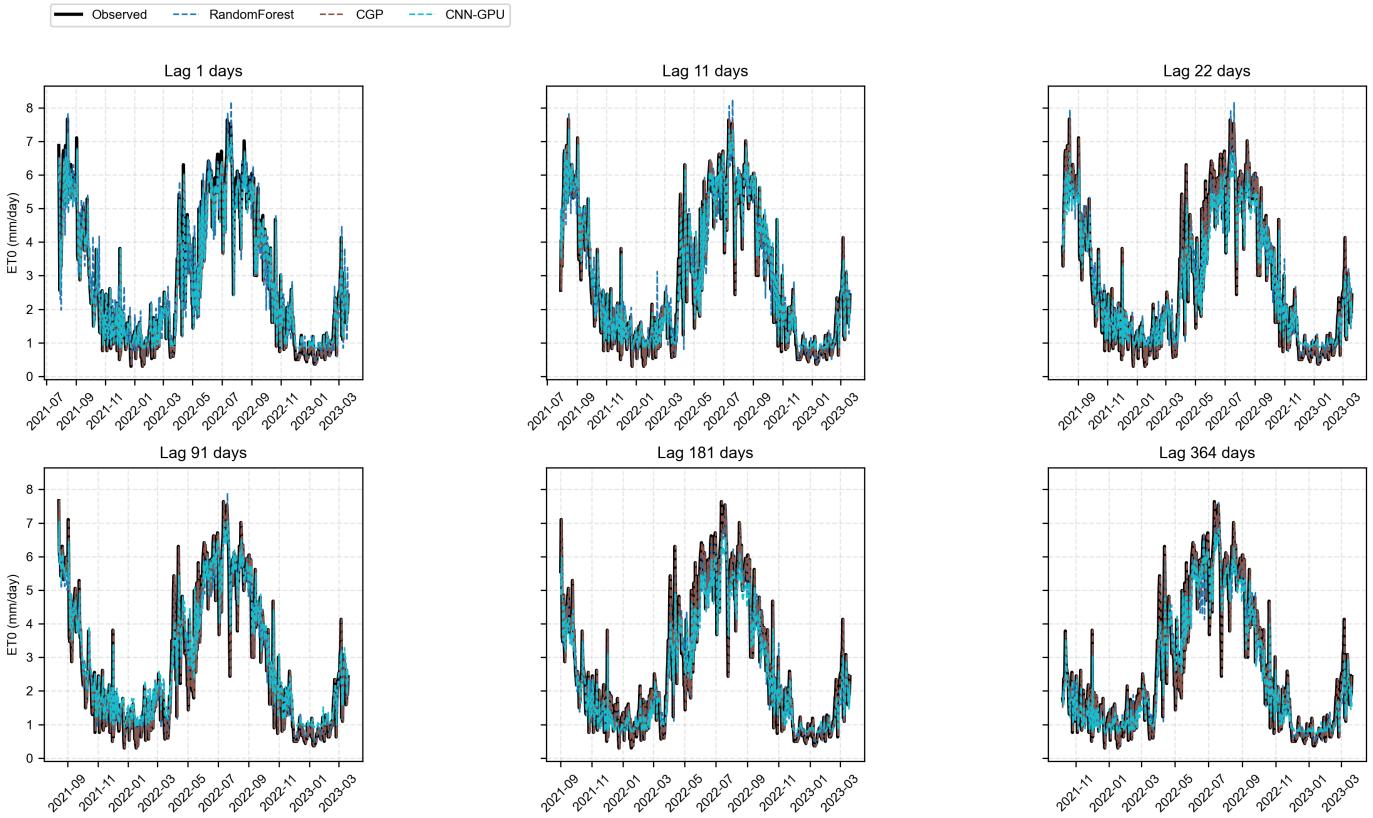


Figure 4. Comparing time series of ET_o forecasts with actual values.

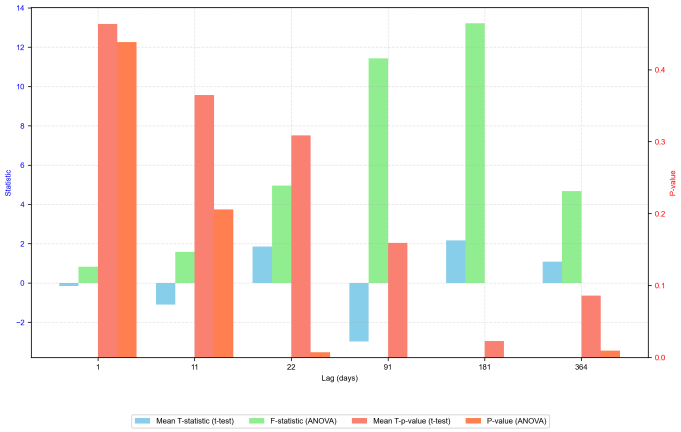


Figure 5. Results of t and F statistical tests for comparing prediction models.

significant differences across most lags (e.g., p=0.477 at 91 days), suggesting closer performance between these two methods.

The F-tests consistently indicated no significant differences in variance across all lags (p-values > 0.05, F-statistics near 1), implying similar dispersion in predictions among the methods. The ANOVA results highlighted that significant performance differences among the three methods became more pronounced at longer lags (22 days and beyond), representing the impact of method selection on prediction accuracy for extended forecasts. Overall, CNN-GPU demonstrated a consistent edge at shorter (1 and 11 days) and very long lags (364 days), while RF performed robustly at intermediate lags (91 and 181 days). These findings suggest that CNN-GPU and RF are reliable choices for ET_o prediction, with CNN-GPU being particularly effective for short-term and long-term forecasts.

3.5 Analysis of the distribution of forecast errors at different time intervals

Figure 6 presents violin plots illustrating the distribution of forecast errors for the applied models. The width of each violin reflects the error density, while the central box plot indicates the median and interquartile range (IQR).

RF demonstrated the most stable performance across all intervals, with the smallest error ranges and distributions consistently centered around zero, making it the most reliable for predicting ET_o. CGP exhibited the greatest instability, with error dispersion escalating at longer lags, reaching a range of $\pm$3.31 at Lag 364. CNN-GPU showed intermediate performance, with wider errors than RF but less variability than CGP. These findings highlight Random Forest's consistent stability for ET_o forecasting across

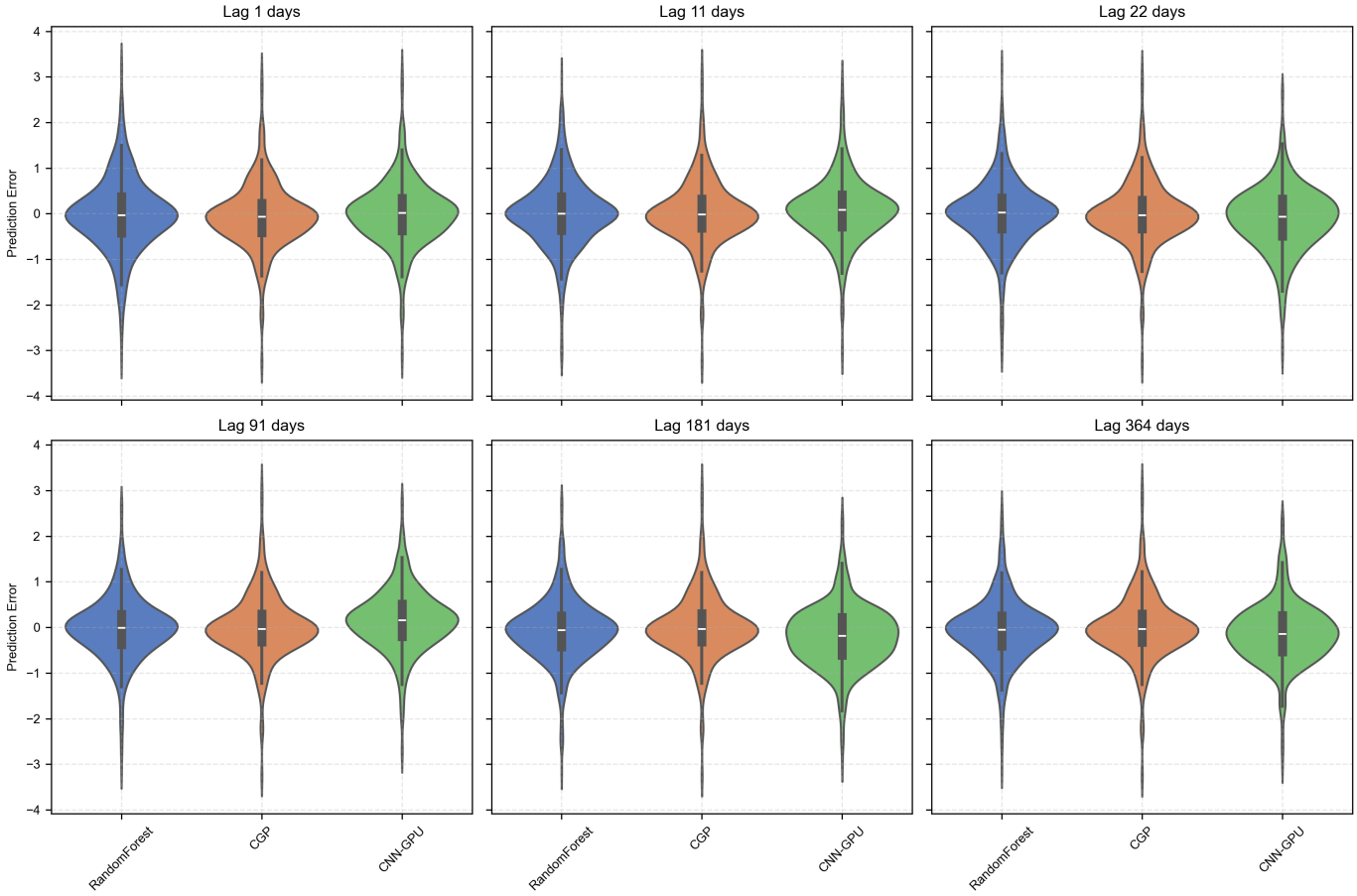


Figure 6. Violin diagrams of the distribution of forecast errors over time intervals.

various time horizons, particularly at intermediate lags, and CNN-GPU's strong performance at short and very long lags, while CGP exhibits increasing inaccuracy at extended timescales.

3.6 Performance analysis of ET_o prediction methods at the 364-day lag

Figure 7 displays the mean forecasts and 95% confidence intervals of the models for the period from October 2021 to March 2023. All methods exhibit similar seasonal patterns with a peak in mid-2022. CGP has the highest mean forecast (maximum 7.64 mm/day), followed closely by RF (maximum 7.56 mm/day), while CNN-GPU has a lower maximum mean forecast (6.88 mm/day). However, RF demonstrates greater precision with a confidence interval width of 2.68 mm/day, compared to CGP's wider interval of 2.74 mm/day, though CNN-GPU has the narrowest interval at 2.61 mm/day. All methods produce unrealistic negative values at their lower bounds, with CGP showing the most extreme negative value (-1.12 mm/day), followed by RF (-0.92 mm/day), and CNN-GPU (-0.57 mm/day). Despite CGP's higher maximum forecast, RF strikes a better balance between accuracy and lower uncertainty, while CNN-GPU provides the tightest confidence intervals, indicating the least variability in predictions. Overall, RF offers a strong performance with high accuracy and reasonable consistency, though all methods struggle with physical consistency due to negative lower bounds.

4 Conclusion

This study provides a systematic evaluation of three ET_o forecasting methods—RF, CGP, and CNN-GPU—across forecasting horizons from 1 to 364 days under semi-arid conditions. The principal findings are as follows. RF demonstrated the most consistent performance across all timescales, maintaining the tightest error distributions and narrowest confidence intervals. Its ability to capture complex nonlinear relationships and seasonal patterns without hyperparameter sensitivity makes it particularly suitable for operational water management applications. CNN-GPU achieved superior accuracy at both the shortest (1 and 11 days) and longest (364 days) horizons, with the lowest overall RMSE of 0.678 mm/day at

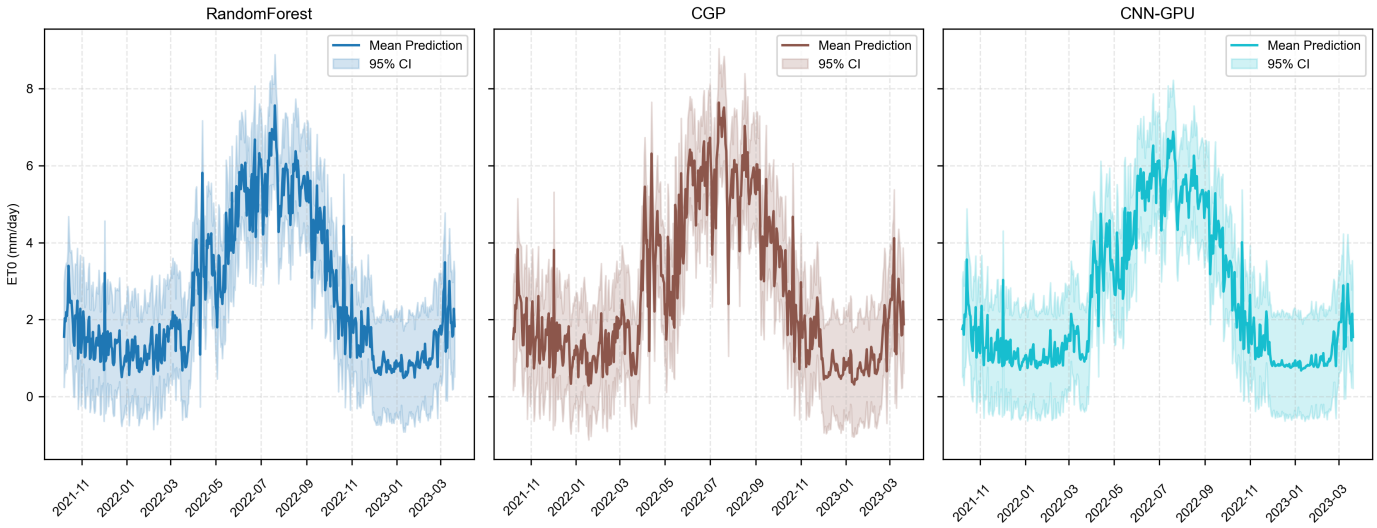


Figure 7. Average ET_o forecasts and 95% confidence interval over a 364-day period.

364 days, suggesting that its hierarchical feature extraction confers an advantage at extremes of the forecasting range. CGP performed competitively at shorter intervals but exhibited progressively wider error distributions and increasing instability at extended lags, limiting its utility for long-range ET_o forecasting in large-scale water management contexts. Statistical analyses (t-tests, F-tests, and ANOVA) confirmed that inter-method differences become statistically significant at lags of 22 days and beyond ($p < 0.05$), underscoring the importance of method selection when extended forecasting accuracy is required. A shared limitation across all three methods is the occasional generation of physically inconsistent negative ET_o predictions at confidence interval lower bounds. This is particularly consequential for operational irrigation scheduling, where negative values are physically impossible and would require post-processing correction before deployment. Potential remedies include setting negative outputs to zero as a post-processing step, or incorporating non-negativity constraints directly into model architectures via activation functions such as ReLU or Softplus. Future work should explore hybrid architectures such as CNN-LSTM to jointly capture local temporal features and long-range dependencies, and should incorporate advanced uncertainty quantification methods—including Bayesian deep learning and quantile regression—to provide calibrated confidence intervals for risk assessment in hydrology and precision agriculture.

Data Availability Statement

Data will be made available on request.

Funding

This work was supported without any funding.

Conflicts of Interest

The authors declare no conflicts of interest.

Ethical Approval and Consent to Participate

Not applicable.

References

[1] Allen, R. G., Pereira, L. S., Raes, D., & Smith, M. (1998). Crop evapotranspiration—Guidelines for computing crop water requirements—FAO Irrigation and drainage paper 56. *FAO, Rome, 300*(9), D05109. Retrieved from https://www.fao.org/3/x0490e/x0490e00.htm

[2] Sadeghzadeh, M., Shiri, J., Karimi, S., & Majnooni, A. (2024). Analysis of factors affecting evapotranspiration zoning. *Environmental Science and Pollution Research, 31*(29), 42295–42313. [Crossref]

[3] Djaman, K., Balde, A. B., Sow, A., Muller, B., Irmak, S., N'Diaye, M. K., ... & Saito, K. (2015). Evaluation of sixteen reference evapotranspiration methods under sahelian conditions in the Senegal River Valley. *Journal of Hydrology: Regional Studies, 3*, 139–159. [Crossref]

[4] Sentelhas, P. C., Gillespie, T. J., & Santos, E. A. (2010). Evaluation of FAO Penman–Monteith and alternative methods for estimating reference evapotranspiration with missing data in Southern Ontario, Canada. *Agricultural Water Management, 97*(5), 635–644. [Crossref]

[5] Pereira, L. S., Allen, R. G., Smith, M., & Raes, D. (2015). Crop evapotranspiration estimation with FAO56: Past

and future. *Agricultural Water Management, 147*, 4–20. [Crossref]

[6] Kisi, O., & Guven, A. (2010). Evapotranspiration modeling using linear genetic programming technique. *Journal of Irrigation and Drainage Engineering, 136*(10), 715–723. [Crossref]

[7] Mehdizadeh, S., Behmanesh, J., & Khalili, K. (2017). Using MARS, SVM, GEP and empirical equations for estimation of monthly mean reference evapotranspiration. *Computers and Electronics in Agriculture, 139*, 103–114. [Crossref]

[8] Karimi, S., Sadraddini, A. A., Nazemi, A. H., Xu, T., & Fard, A. F. (2018). Generalizability of gene expression programming and random forest methodologies in estimating cropland and grassland leaf area index. *Computers and Electronics in Agriculture, 144*, 232–240. [Crossref]

[9] Shiri, J. (2019). Modeling reference evapotranspiration in island environments: Assessing the practical implications. *Journal of Hydrology, 570*, 265–280. [Crossref]

[10] e Lucas, P. D. O., Alves, M. A., e Silva, P. C. D. L., & Guimaraes, F. G. (2020). Reference evapotranspiration time series forecasting with ensemble of convolutional neural networks. *Computers and Electronics in Agriculture, 177*, 105700. [Crossref]

[11] Ferreira, L. B., & da Cunha, F. F. (2020). Multi-step ahead forecasting of daily reference evapotranspiration using deep learning. *Computers and Electronics in Agriculture, 178*, 105728. [Crossref]

[12] Koza, J. R. (1992). *Genetic Programming: On the Programming of Computers by Means of Natural Selection*. MIT Press, Cambridge, MA.

[13] Garcia-Garcia, C., Morales-Reyes, A., & Escalante, H. J. (2023). Continuous Cartesian Genetic Programming based representation for multi-objective neural architecture search. *Applied Soft Computing, 147*, 110788. [Crossref]

[14] Herath, H. M. V. V., Chadalawada, J., & Babovic, V. (2021). Genetic programming for hydrological applications: to model or to forecast that is the question. *Journal of Hydroinformatics, 23*(4), 740–763. [Crossref]

[15] Shiri, J., Kişi, Ö., Landeras, G., López, J. J., Nazemi, A. H., & Stuyt, L. C. (2012). Daily reference evapotranspiration modeling by using genetic programming approach in the Basque Country (Northern Spain). *Journal of Hydrology, 414*, 302–316. [Crossref]

[16] Breiman, L. (2001). Random forests. *Machine Learning, 45*(1), 5–32. [Crossref]

[17] Ao, Y., Li, H., Zhu, L., Ali, S., & Yang, Z. (2019). The linear random forest algorithm and its advantages in machine learning assisted logging regression modeling. *Journal of Petroleum Science and Engineering, 174*, 776–789. [Crossref]

[18] Tyralis, H., Papacharalampous, G., & Langousis, A. (2019). A brief review of random forests for water scientists and practitioners and their recent history in water resources. *Water, 11*(5), 910. [Crossref]

[19] Miller, J. F. (2020). Cartesian genetic programming: its status and future. *Genetic Programming and Evolvable Machines, 21*(1), 129–168. [Crossref]

[20] Miller, J. F., & Harding, S. L. (2009, July). Cartesian genetic programming. In *Proceedings of the 11th Annual Conference Companion on Genetic and Evolutionary Computation Conference: Late Breaking Papers* (pp. 3489–3512). [Crossref]

[21] Miller, J., & Turner, A. (2015, July). Cartesian genetic programming. In *Proceedings of the Companion Publication of the 2015 Annual Conference on Genetic and Evolutionary Computation* (pp. 179–198). [Crossref]

[22] Ahmad, M. W., Mourshed, M., & Rezgui, Y. (2017). Trees vs Neurons: Comparison between random forest and ANN for high-resolution prediction of building energy consumption. *Energy and Buildings, 147*, 77–89. [Crossref]

[23] Cutler, A., Cutler, D. R., & Stevens, J. R. (2012). Random forests. In *Ensemble Machine Learning* (pp. 157–175). Springer, New York, NY. [Crossref]

[24] LeCun, Y., Bengio, Y., & Hinton, G. (2015). Deep learning. *Nature, 521*(7553), 436–444. [Crossref]

[25] Metropolis, N., & Ulam, S. (1949). The Monte Carlo method. *Journal of the American Statistical Association, 44*(247), 335–341. [Crossref]

[26] Helsel, D. R., Hirsch, R. M., Ryberg, K. R., Archfield, S. A., & Gilroy, E. J. (2020). Statistical methods in water resources. *Techniques and Methods, Book 4, Chapter A3*. U.S. Geological Survey. [Crossref]